Electronic Supplementary Material (ESI) for Physical Chemistry Chemical Physics

Structural prediction of a rhodamine-based biosensor and comparison with biophysical data

Marcos Brown Gonçalves, [a] Jens Dreyer, [a] Paola Lupieri, [a] Claudia Barrera – Patiño, [a] Emiliano Ippoliti, [a] Martin R. Webb, [b] John E. T. Corrie, [b] and Paolo Carloni [a]

[a] *Computational Biophysics, German Research School for Simulation Sciences,D-52425 Jülich, Germany and Institute for Advanced Simulation, Forschungszentrum Jülich, D-52425 Jülich, Germany.*
[b] *MRC National Institute for Medical Research, The Ridgeway, Mill Hill, London, NW7 1AA, United Kingdom.*

Supplementary information

1- RMSD and Clustering analysis

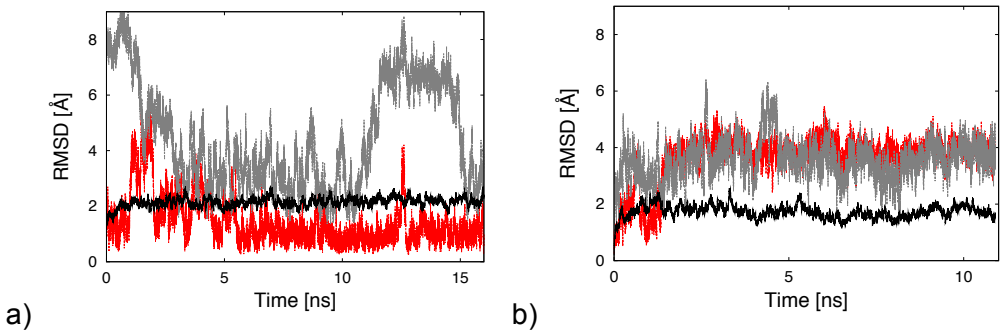

Figure S-1 Root mean square deviation (RMSD) versus simulated time of the phosphate binding protein (PBP) backbone (black) and the rhodamine fluorophore residues RHO197 (red) and RHO17 (grey) for a) RHO_2−PBP·Pi and b) RHO_2−PBP.

The root mean square deviations (RMSDs) of the phosphate binding protein (PBP) backbones fluctuate around an average values after 3 ns, suggesting that the overall structures are equilibrated after this time (Fig. S-1). The RMSD of the two rhodamine fluorophores (RHO) in RHO_2−PBP fluctuates less than the corresponding one in RHO_2−PBP·Pi, which contains inorganic phosphate (Pi) bound to PBP. This is consistent with the fact that in RHO_2−PBP the two fluorophores maintain a quite stable stacked dimer conformation (Fig. 4b, which shows a representative of the most populated cluster from the classical molcecular dynamics (MD) simulation for RHO_2−PBP), whereas in RHO_2−PBP·Pi they experience large conformational flexibility (Fig. 4a, which shows a representative of the most populated cluster from the classical MD simulation for RHO_2−PBP·Pi).

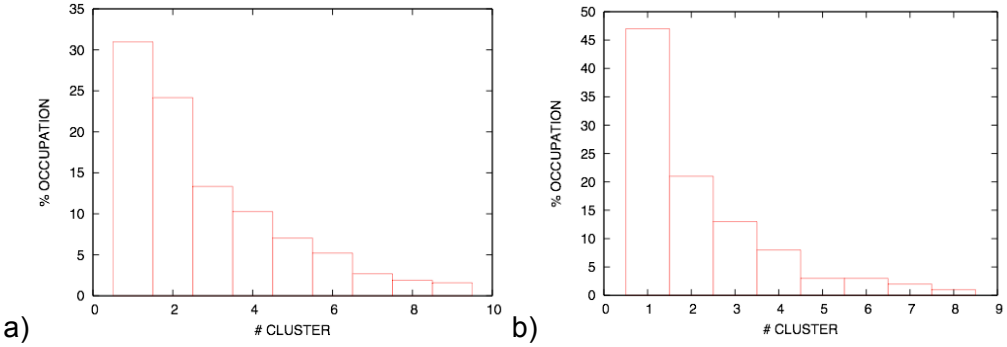

Figure S-2 Cluster analysis of classical MD of RHO_2−PBP·Pi (a) and RHO_2−PBP (b). The percentage of occupation versus number of cluster is reported.

The clustering analyses were carried out using a Gromacs tool as described in Daura et al. [Daura99] with a cutoff criterion of 0.14 nm RMSD. The occupation percentages for the RHO_2−PBP·Pi form are distributed more homogeneously than those of RHO_2−PBP (Fig S-2). In particular, the sum of occupation percentages for clusters 1-2 in RHO_2−PBP·Pi is about 60%. RHO_2−PBP has one cluster with an occupation larger than 45% and the sum of occupation percentages for clusters 1-2 is around 70%. These results are consistent with the fact that RHO_2−PBP·Pi exhibits more structural flexibility than RHO_2−PBP (Fig. 4, Ch. 3.1 and 3.2, Figs. S-4 – S-7).

2- Circular dichroism (CD) spectra

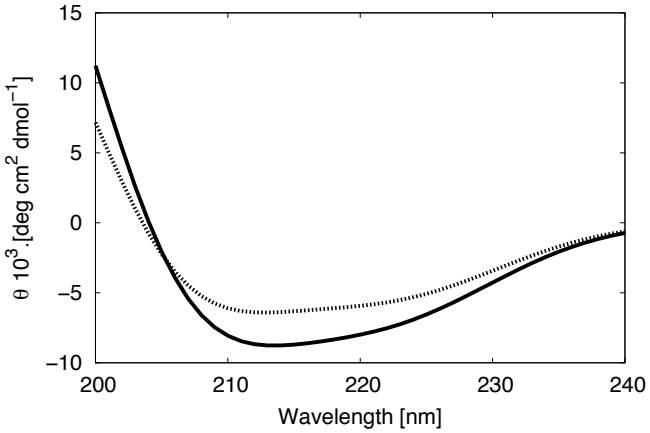

Figure S-3 Simulated CD spectra for RHO_2−PBP (solid line) and RHO_2−PBP·Pi (dashed line). CD spectra were computed by averaging results from 20 snapshots equally separated from the MD trajectory. The spectra were calculated using the web interface developed by Hirst et al. [Bulheller07, Bulheller09] with parameters derived ab initio [Besley99].

3- Pi coordination

The partial charges for the Pi compound were calculated following the RESP procedure [Bayly93] based on gas phase DFT calculations of a reduced model (licorized residues in Fig. 3). The following partial charges were used for the $[H_2PO4]^-$ anion: +1.41 *e* for phosphorus, -0.72 *e* for oxygen, -0.90 *e* for oxygen bound to hydrogen and +0.42 *e* for hydrogen atoms.

Several residues interact with Pi during the classical MD (Tab. S-1, Fig. 3 and Fig. S-4). Specifically, the NH_2 groups of ARG135 interact with O1 of Pi (Figs. S-4 a,f). OH@SER139, NH@THR141, OG@THR141 and NH@GLY140 interact with O2 of Pi (Figs. S-4b,c,e,g). OH@SER38 interacts with O3 of Pi (Figs. S-4d,h). Finally, ASP56 side chain binds with O3H and O4H (Figs. S-4i,j).

Table S-1 Coordination of Pi in RHO_2–PBP·Pi: Crystal structure and selected average distances (with standard deviation). (a) X-Ray data from Ref. [WANG97].

	Xray[a] [Å]	Simulation [Å]
Pi:O1-THR10:N	2.77	4.92±0.98
Pi:O1-THR10:OG1	2.64	5.09±1.42
Pi:O1-ARG135:NH2	2.85	2.85±0.14
Pi:O1-ARG135:NH1	-	3.11±0.35
Pi:O2-ARG135:NH1	2.84	-
Pi:O2-SER139:OG	2.67	2.45±0.06
Pi:O2-THR141:N	2.87	3.09±0.22
Pi:O2-THR141:OG	2.68	3.38±0.34
Pi:O2-GLY140:N	-	3.03±0.17
Pi:O3-GLY140:N	2.73	-
Pi:O3-SER38:N	2.67	3.49±0.31
Pi:O3-SER38:OG	2.73	3.43±0.38
Pi:O3-ASP56:OD1	-	2.58±0.12
Pi:O4-ASP56:OD2	2.43	2.54±0.08
Pi:O4-PHE11:N	2.81	4.53±0.73

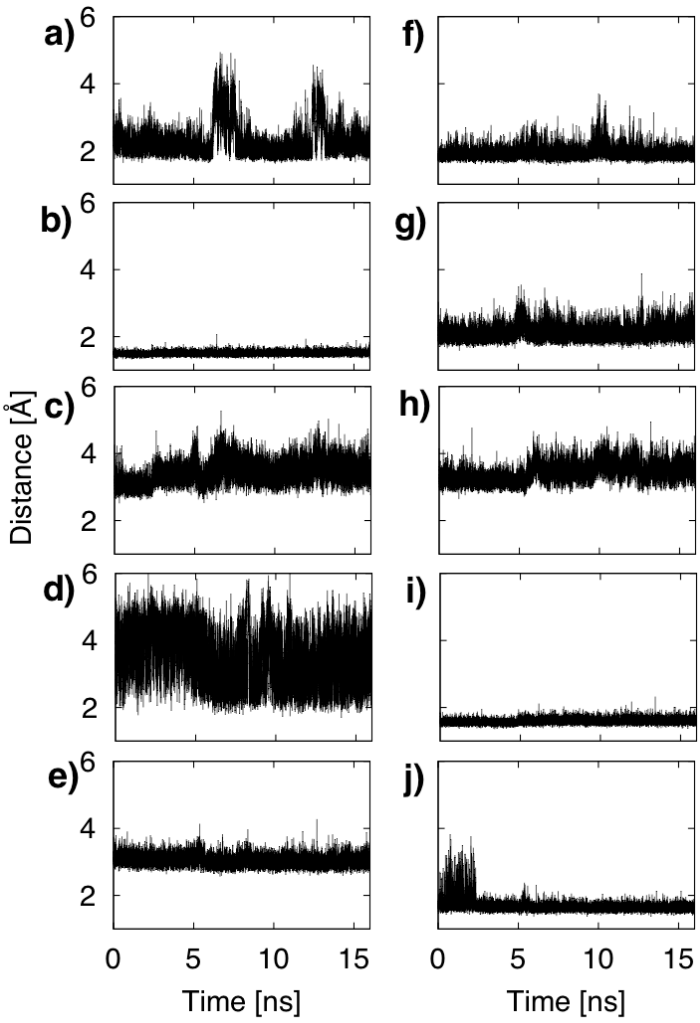

Figure S-4 Time evolution of the hydrogen bond distances for Pi:O1-ARG135:NH_2 a), Pi:O2-SER139:OG b), Pi:O2-THR141:OG c), Pi:O3-SER38:OG d), Pi:O2-GLY140:N e), Pi:O1-ARG135:NH_2 f), Pi:O2-THR141:N g), Pi:O3-SER38:N h), Pi:O3H-ASP56:OD2 i), Pi:O4H-ASP56:OD1 j), distances plotted as a function of time. Labeling as in Fig. 3 in the main text.

4- Rhodamine fluorophores

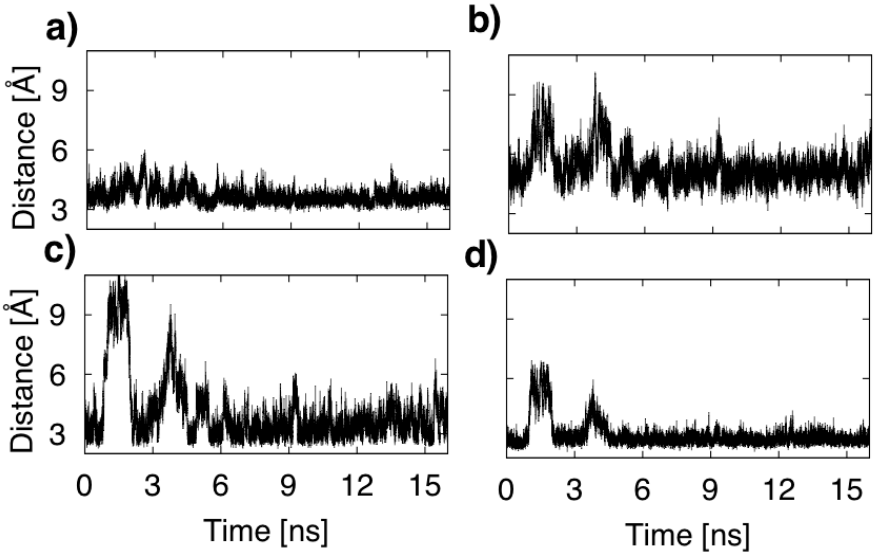

Figure S-5 RHO_2–PBP·Pi: Distances of RHO197:C-LEU291:O a), RHO197:C-ASN202:H b), RHO197:O-ASN203:C c), RHO197:N-GLN201:O d), plotted as a function of simulated time (cf. Fig. 4a in the main text).

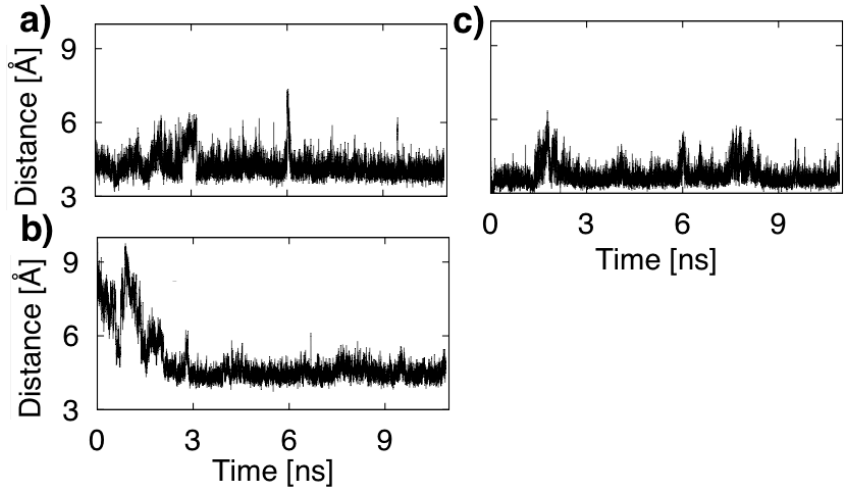

Figure S-6 RHO_2–PBP: Distances of RHO197(C)-Leu291(C) a), RHO197-TYR198 b), and RHO197(C)-Leu291(O) c), plotted as a function of simulated time (cf. Fig. 4a in the main text).

The average RHO-RHO distances are around 4.2±0.8, 4.4±0.7 and 5.0±0.7 Å, showing a tilted π-π interaction and the normal angles between xanthylium rings are around 22.6±10.6. In the first half of the trajectory, the distances and the normal angle fluctuate from 4 to 9 Å and 0˚ to 70˚, respectively. At around 2.5 and 4.5 ns the RHO moieties almost disconnect from each other with RHO17-RHO197 separations of ~ 7-9 Å. After 5 ns, the π-π stacking maintains a stable relationship with a distance of 3.7-4.8 Å and a normal angle of around 20˚ showing a fairly coplanar configuration.

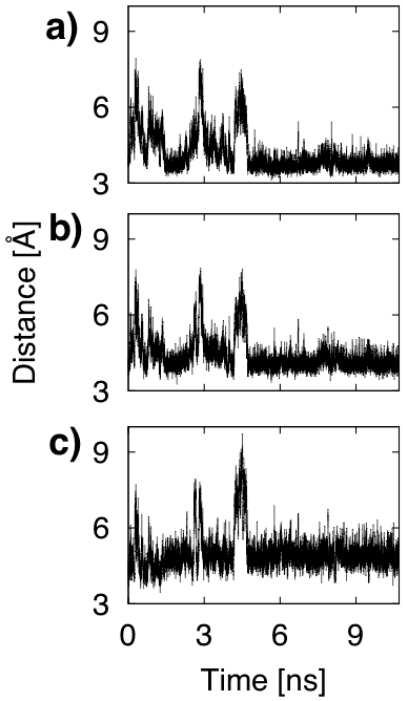

Figure S-7 Distances between RHO17 – RHO197 in RHO_2–PBP measured between each of the geometrical centres of the corresponding pairs of rings in the xanthylium moieties. See Fig. S-10 for the labeling of the individual rings.

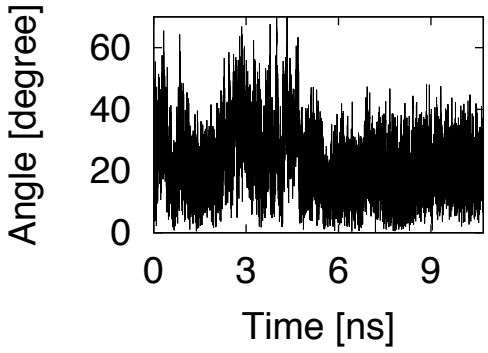

Figure S-8 Angle between vectors normal to the xanthylium rings of RHO17-RHO197 in RHO2−PBP as shown in Fig. S-10. The angle describes the mutual orientation of the two xanthylium rings. For a fully parallel configuration, i.e. ideal π-π stacking, the angle is 0^o.

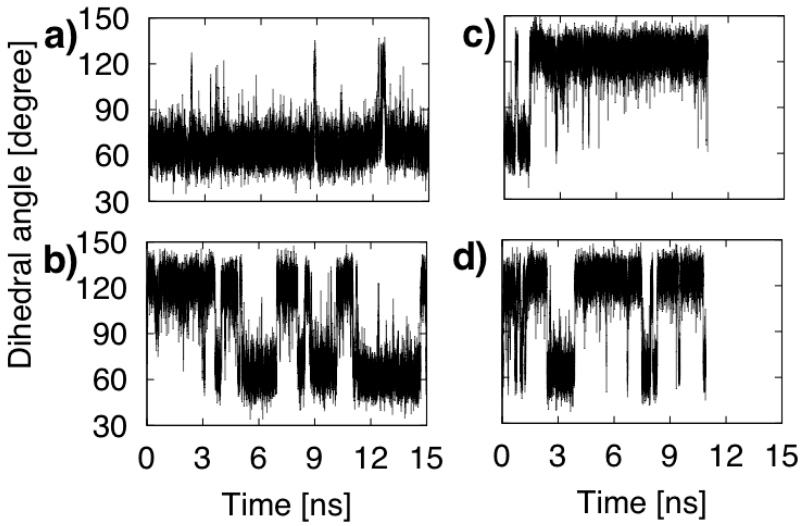

Figure S-9 Dihedral angles between the xanthylium system and the aryl ring for each rhodamine in RHO2−PBP.Pi for (a) RHO197 and (b) RHO17. In RHO2−PBP for (c) RHO197 and (d) RHO17.

For the RHO_2−PBP·Pi system, the dihedral angle between the xanthylium and the aryl group in RHO197 stays stable during more than 95 % of the trajectory at around 65˚ (Fig. S-9a). On the other hand, RHO17 oscillates between 125˚ and 65˚ (Fig S-9b). In RHO_2−PBP system, the dihedral angle between xanthylium and aryl group in the RHO197 stays stable at 130˚ with the exception of the first 1.5 ns, where the dihedral angle fluctuates between 70˚ and 130˚ (Fig. S-9c). The RHO197 stability is due to the larger close contact interaction with the protein that maintains the RHO197 more tightly bound to the protein. On the other hand, RHO17 shows a larger flexibility although it is also oscillating between two values, i.e. 65˚ and 130˚ (Fig. S-9d).

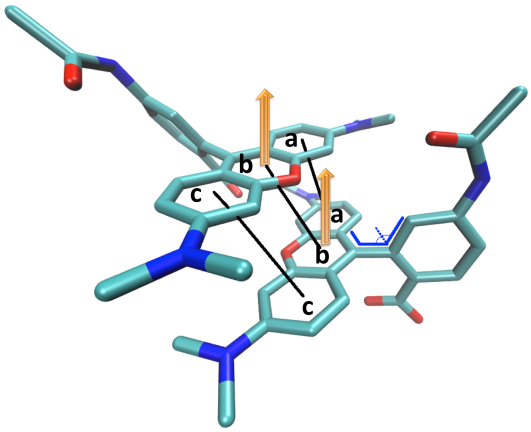

Figure S-10 Schematic representation of the calculations shown in Figs. S-7 to S-9 for RHO_2−PBP. In black, distances between the geometric centres of the "aa", "bb" and "cc" pairs of rings (Fig. S-7). Orange arrows represent the normal vector of the xanthylium moieties (Fig. S-8). In blue, dihedral angle between xanthylium plane and aryl ring (Fig. S-9).

5- Orbitals and electronic transitions

Fig. S-11 shows representative Kohn-Sham molecular orbitals (MOs) for the 3,6-bis(dimethylamino)xanthylium cation in the RHO_2−PBP·Pi system. Analysis of the spectrum simulated for RHO_2−PBP·Pi (Fig. 5) based on 80 snapshots (40 snapshots for each xanthylium cation moiety) shows that the individual spectra can be divided into 3 groups with different patterns. One group exhibits only a single

dominant transition, namely the π→π* HOMO→LUMO transition. A second group shows two transitions of significant intensity. One of them is HOMO→LUMO transition; the other one corresponds to the HOMO-1→LUMO excitation, with the latter being less intense. The third group shows a pattern with two or three transitions of mixed character, mainly of the previous mentioned transitions, though with lower relative intensities as compared to the other two groups. The intense HOMO→LUMO transition is spread in between 440 nm to 480 nm peaking around 450 nm. The second most intense contribution, mainly π→π* HOMO-1→LUMO, is even more dispersed from 425 nm to 470 nm.

Fig. S-12 shows representative Kohn-Sham MOs for the two stacked xanthylium cations in the RHO_2−PBP system. The shape and character of the MOs is well preserved for different snapshots along the trajectory. Two groups with patterns containing one or two higher transitions are identified to contribute to the calculated absorption spectrum of RHO_2−PBP (Fig. 5). The group with only a single intense transition is mainly due to the combination of HOMO-1→LUMO transition and HOMO→LUMO+1. The second group exhibits two or three transitions with significant intensities, partially corresponding to the previously mentioned transitions in combination with the HOMO-2→LUMO+1 transition, but in other snapshots to the HOMO-3→LUMO. In some snapshots small transition intensities are found near 490 nm. These transitions are assigned as HOMO-1→LUMO and HOMO→LUMO+1 in different combinations.

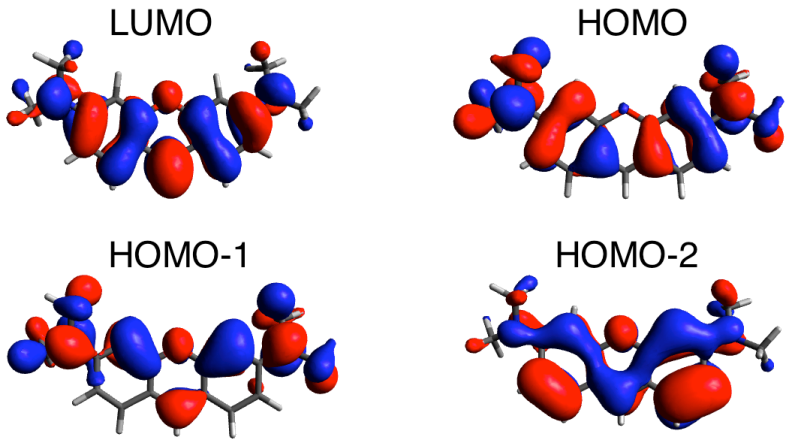

Figure S-11 RHO_2–PBP·Pi: the three highest occupied MOs (HOMO-2, HOMO-1, HOMO) Kohn-Sham molecular orbitals (MOs) of the xanthene moiety (upper panel of Fig. 1, in red) of the rhodamine chromophores, along with the lowest unoccupied MO (LUMO). All orbitals have π or π* character, respectively.

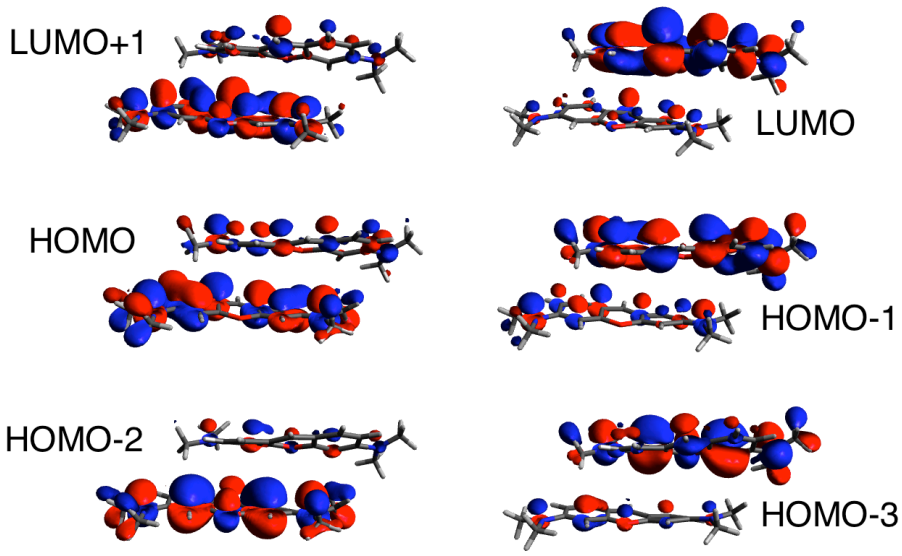

Figure S-12 RHO_2–PBP: the four highest occupied MOs (HOMO-3, HOMO-2, HOMO-1, HOMO) Kohn-Sham molecular orbitals (MOs) of the stacked xanthene moieties of the rhodamine chromophores, along with the lowest unoccupied MO (LUMO, LUMO+1). All orbitals have π or π* character, respectively.

Bibliography

[Bulheller07] B. M. Bulheller, A. Rodger and J. D. Hirst, *Phys. Chem. Chem. Phys*., 2007, **9**, 2020–2035.
[Bulheller09] B. M. Bulheller and J. D. Hirst, *Bioinformatics*, 2009, **25**, 539–540.
[Besley99] N. A. Besley and J. D. Hirst, *J. Am. Chem. Soc*., 1999, **121**, 9636–9644.
[Daura99] X. Daura, K. Gademann, B. Jaun, D. Seebach, W. F. van Gunsteren and A. E. Mark, *Angew. Chem. Int. Ed*., 1999, **38**, 236–240.
[Bayly93] C. Bayly, P. Cieplak, W. Cornell and P. Kollman, *J. Phys. Chem*., 1993, **97**, 10269–10280.
[Wang97] Z. Wang, H. Luecke, N. Yao and F. A. Quiocho, *Nat Struct Mol Biol*, 1997, **4**, 519–522.